

Evaporative cooling of reactive polar molecules confined in a two-dimensional geometry

Bihui Zhu¹, Goulven Quéméner², Ana M. Rey^{1*} and Murray J. Holland^{1†}

¹*JILA and Department of Physics, University of Colorado, 440 UCB, Boulder, CO 80309, USA and*

²*Laboratoire Aimé Cotton, CNRS, Université Paris-Sud,*

ENS Cachan, Campus d'Orsay, Bât. 505, 91405 Orsay, FRANCE

(Dated: February 8, 2022)

Recent experimental developments in the loading of ultracold KRb molecules into quasi-two-dimensional traps, combined with the ability to tune the ratio between elastic and loss (inelastic/reactive) collisions through application of an external electric field, are opening the door to achieving efficient evaporative cooling of reactive polar molecules. In this paper, we use Monte Carlo simulations and semianalytic models to study theoretically the experimental parameter regimes in which evaporative cooling is feasible under current trapping conditions. We investigate the effect of the anisotropic character of dipole-dipole collisions and reduced dimensionality on evaporative cooling. We also present an analysis of the experimentally relevant anti-evaporation effects that are induced by chemical reactions that take place when more than one axial vibrational state is populated.

PACS numbers: 34.50.Cx, 37.10.Mn, 05.20.Dd

I. INTRODUCTION

Polar molecules that exhibit strong dipole-dipole interactions provide a flexible platform for realizing a broad range of interesting phenomena relevant to condensed matter physics, quantum information sciences and precision measurements [1–7]. The parameter regime of interest is generally ultralow temperature and high phase-space density, where novel quantum features can emerge. In practice, it turns out to be difficult to cool molecules into the desired regime using standard methods due to their complicated internal level structure. In the past few years, significant experimental progress has been made towards this goal through the demonstration of a method for preparing a gas of fermionic KRb molecules in the lowest electronic, vibrational, and rotational quantum state, with a temperature T at the verge of quantum degeneracy (*i.e.* $T/T_F \sim 1$ where T_F is the Fermi temperature) [8–10]. From this starting point, one would like to further increase the phase-space density by implementing evaporative cooling—demonstrated to be one of the most useful cooling methods for quantum gases [11–13].

A fundamental limitation to the effectiveness of evaporative cooling for polar molecules is their fast losses. For KRb molecules, the losses arise mainly from exothermic chemical reactions, *i.e.* $\text{KRb} + \text{KRb} \rightarrow \text{K}_2 + \text{Rb}_2$. In such reactions, molecules prepared in different internal states can undergo barrierless collisions, with a lifetime of only ~ 10 ms [10, 14]. In contrast, identical fermionic KRb molecules at ultra-low temperature are protected by the p -wave barrier, which potentially results in a much slower reaction rate [10]. However, due to the anisotropic nature of the dipole-dipole interaction, molecules of the correct orientation can be attracted towards each other by experiencing “head-to-tail” collisions. As a result, the p -wave barrier can be lowered by the application of a strong external field, increasing the loss mechanism of the molecules.

Significantly, these obstacles can be overcome by confining the molecules into quasi-two-dimensional traps, which can be generated by a one-dimensional optical lattice. In this case, the adverse collisions can be greatly suppressed and the reaction barrier effectively raised [15–17]. Furthermore, both the elastic and reactive collision rates can be tuned by controlling the applied external electric field and the trapping potential. Thus, while most previous experiments implementing evaporative cooling were performed in three-dimensional geometries [18], here we are explicitly interested in focussing on evaporative cooling in two-dimensions, with the anisotropic collisions that arise from the dipolar interaction. A detailed understanding of this situation would be beneficial for future experimental realizations.

Given this motivation, we theoretically investigate evaporative cooling of molecules. We use both Monte Carlo (MC) simulations and models developed on the basis of kinetic theory to study the efficiency of evaporative cooling with parameters applicable to current state-of-the-art KRb experiments. The paper is structured as follows. In Sec. II we explore the effect of anisotropic collisions on evaporative cooling. In Sec. III we consider the effect of reduced trap dimension, *i.e.* two-dimensional rather than three-dimensional traps. In Sec. IV we apply the MC method to determine the optimum evaporative cooling trajectory for KRb molecules. In Sec. V we discuss the potential anti-evaporation mechanism arising from the energy dependence of the reactive loss.

II. EVAPORATIVE COOLING WITH ANISOTROPIC COLLISIONS

A. Anisotropic elastic collisions between polar molecules

Evaporative cooling relies on removing particles with above-average energy and redistributing the residual energy among the remaining particles by elastic collisions so that the temperature falls. For polar molecules, the characteristic parameters that encapsulate the elastic scattering process can be dramatically modified by the application of external fields. In

* arey@jilau1.colorado.edu

† murray.holland@colorado.edu

| E_c (nK) | a | a' | α | α' | $\lambda(10^{-6}\text{cm})$ |
|------------|------|--------|----------|-----------|-----------------------------|
| 1 | 0.31 | 0.0005 | 1.00 | 2.19 | 0.38 |
| 10 | 0.27 | 0.06 | 1.00 | 2.09 | 3.67 |
| 100 | 0.24 | 0.21 | 1.19 | 7.03 | 5.99 |
| 1000 | 0.34 | 0.40 | 2.47 | 26.40 | 3.42 |

TABLE I. Derived parameters from the fit of Eq. (1) for the scattering energies shown in FIG. 1.

the presence of an external electric field, the dipole-dipole interaction between polar molecules can mix different partial waves and give rise to highly-anisotropic scattering. Moreover, for identical fermions, the lowest total angular momentum partial wave that has the correct symmetry is p -wave, so the elastic collisions are anisotropic at ultralow temperature even in the absence of applied fields [19].

Considering current experimental conditions [15], we have computed the differential and total scattering cross-section for KRb molecules in two-dimensions at an induced dipole moment $d = 0.2$ debye as a function of the collision energy E_c . The theoretical formalism is explained in Appendix A. FIG. 1(a) shows the dependence of differential cross-section on the scattering angle, ϕ , which is the precession angle of the relative momentum during the collision. Scattering is mainly forward (0 or 2π) and backward (π) after a collision. The peak is more pronounced as the collision energy increases due to the larger contribution of higher partial waves. This differential cross-section is well parametrized by the empirical function

$$\left(\frac{d\lambda(\phi)}{d\phi}\right)_{E_c} = \lambda(E_c) \left(a(\cos\phi)^{2\alpha} + a'(\cos\phi)^{2\alpha'} \right), \quad (1)$$

with a , a' , α and α' constants that are real and positive, and with the total cross-section [20] given by

$$\lambda(E_c) = \int_0^{2\pi} d\phi \left(\frac{d\lambda(\phi)}{d\phi}\right)_{E_c}. \quad (2)$$

The dependence of λ on collision energy E_c is shown in FIG. 1(b). Our best parametrization for various scattering energies is given in Table I. Note that at $E_c \sim 1$ nK, the angular dependence of the differential cross-section is well described by that of the lowest odd partial wave (see Appendix. A), since $a \gg a'$ and $\alpha \approx 1$.

B. Thermalization rate

The thermalization rate characterizes the timescale needed for a system to redistribute energy after an evaporative cut. To quantitatively investigate the thermalization under anisotropic collisions, we adopt the typical experimental procedure of cross-dimensional thermalization [21, 22]. In order to isolate the effect of anisotropic elastic collisions, we will neglect losses completely, and also neglect the energy dependence in the total elastic cross-section λ for these thermalization calcu-

lations.

Consider a gas of N molecules in a two-dimensional harmonic trap with a slight initial imbalance of temperatures along each axis. This initial condition can be prepared in experiment by parametric heating of an equilibrium gas [21]. We define an effective temperature T_i in the i th direction in terms of the total energy E_i by $k_B T_i = E_i/N = \overline{p_i^2}/(2m) + m\omega_i^2 \overline{x_i^2}/2$, where ω_i is the trapping frequency, m is the molecule mass, and $\overline{p_i^2}/(2m)$ and $m\omega_i^2 \overline{x_i^2}/2$ denote the average kinetic energy and potential energy. We assume that the system is well described by the Boltzmann distribution

$$f_0(\mathbf{x}, \mathbf{p}) = n_0 \exp\left(-\sum_i \left(\frac{p_i^2}{m} + m\omega_i^2 x_i^2\right)/(2k_B T_i)\right), \quad (3)$$

where n_0 guarantees normalization, *i.e.*

$$\frac{1}{(2\pi\hbar)^2} \int d^2x d^2p f_0(\mathbf{x}, \mathbf{p}) = N. \quad (4)$$

Without loss of generality, we assume $T_y = (1 - \xi)T_x$ with $\xi > 0$. Elastic collisions lead to an exchange of energy between the x and y directions and reduce the relative temperature difference. The rate of such change is [23]

$$\begin{aligned} \frac{dE_x}{dt} &= N k_B \frac{dT_x}{dt} = \frac{1}{2m(2\pi\hbar)^4} \int d^2x d^2p_1 d^2p_2 d\phi' \\ &\times f_0(\mathbf{x}, \mathbf{p}_1) f_0(\mathbf{x}, \mathbf{p}_2) |\mathbf{p}_1 - \mathbf{p}_2| \frac{d\lambda(\phi')}{d\phi'} \Delta E_x. \end{aligned} \quad (5)$$

This involves the energy change per collision given by

$$\Delta E_x = \frac{1}{4m} |\mathbf{p}_1 - \mathbf{p}_2|^2 (\cos^2 \phi' - \cos^2 \phi), \quad (6)$$

where ϕ and ϕ' are the angles between the relative momentum and the total momentum before and after the collision respectively. The period of time it takes to thermalize, τ , can be defined as the $1/e$ decay time of the temperature difference, so that

$$\frac{dT_x}{dt} = -\frac{1}{\tau} (T_x - T_0), \quad (7)$$

where $T_0 = (T_x + T_y)/2$ is the temperature at equilibrium. From Eq. (5) and Eq. (7), we obtain the average number of elastic collisions required for the system to thermalize, κ , in the following way. We begin by defining the collision rate γ

$$\gamma = \frac{\lambda}{m(2\pi\hbar)^4} \int d^2x d^2p_1 d^2p_2 f_0(\mathbf{x}, \mathbf{p}_1) f_0(\mathbf{x}, \mathbf{p}_2) |\mathbf{p}_1 - \mathbf{p}_2|, \quad (8)$$

so that $\kappa \equiv \lim_{\xi \rightarrow 0} (\tau\gamma)$, independent of the initial temperature and trapping frequencies [22, 24]. Combining Eq. (3)–Eq. (8) with the form of the differential cross-sections given in Eq. (1) leads to the following result:

$$\kappa = \frac{8}{15\sqrt{\pi}} \left\{ \frac{a}{2\alpha + 2} \frac{\Gamma(\alpha + \frac{1}{2})}{\Gamma(\alpha + 1)} + \frac{a'}{2\alpha' + 2} \frac{\Gamma(\alpha' + \frac{1}{2})}{\Gamma(\alpha' + 1)} \right\}^{-1}.$$

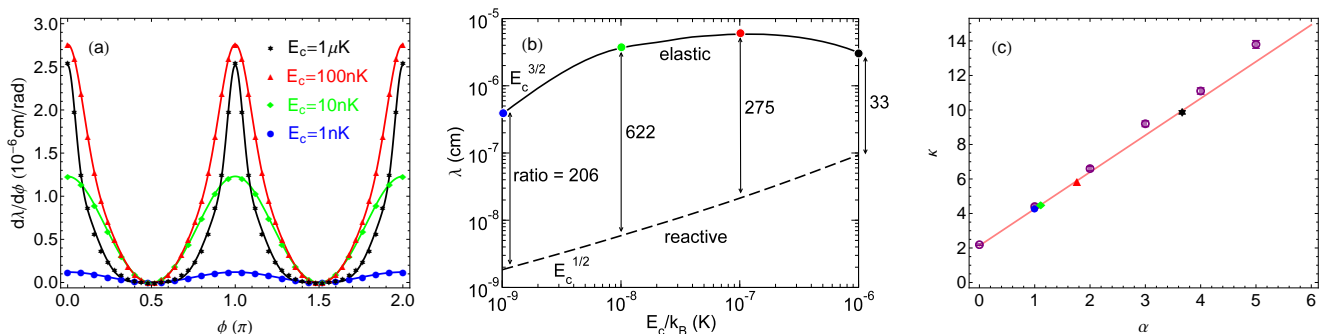


FIG. 1. (Color online) (a) Two-dimensional differential scattering cross-section for elastic collisions as a function of the scattering angle. Four collision energies are shown; $E_c = 1 \text{ nK}$ (blue disk), 10 nK (green diamond), 100 nK (red triangle), and $1 \mu\text{K}$ (black star). The induced dipole moment is $d = 0.2$ debye and the harmonic frequency of the one-dimensional confinement potential is $\nu = 23 \text{ kHz}$. The solid lines show the empirical formula Eq. (1). (b) Total scattering cross-section for elastic collisions (solid line) and reactive processes (dashed line) as a function of the collision energy for an induced dipole moment of $d = 0.2$ debye and a one dimensional confinement of $\nu = 23 \text{ kHz}$. The ratio of elastic to reactive is indicated at four different collision energies; $E_c = 1 \text{ nK}$ (blue point), 10 nK (green point), 100 nK (red point), and $1 \mu\text{K}$ (black point). (c) Number of collisions κ required for thermalization for different differential scattering cross-sections. The magenta solid line shows Eq. (10). The purple circles are results from the MC simulations, and are shown with their small statistical error bars. The four symbols (blue disk, green diamond, red triangle, black star) correspond to the same energies as (a).

(9)

When $a' = 0$ and $\alpha' = 0$, this reduces to the particularly simple expression

$$\kappa = \frac{16}{15}(2\alpha + 2), \quad (10)$$

which corresponds to the differential cross-section

$$\frac{d\lambda(\phi)}{d\phi} = a \cos^{2\alpha}\phi. \quad (11)$$

In order to interpret these results, for each scattering energy E_c , we calculate κ using Eq. (9), and plot the result on the (α, κ) line, as prescribed by Eq. (10), with markers (star, square, triangle, diamond, and disk), as shown in FIG. 1(c). The use of the linear relationship between α and κ is supported by results obtained from MC simulations, as described in Appendix B, utilizing the differential cross-section form of Eq. (11) directly (purple circles). The exception is at large α , where the assumption adopted in deriving Eq. (9)—namely that of a Boltzmann distribution parametrized by an effective temperature—becomes poor when the thermalization is too slow.

The calculations demonstrate a strikingly strong dependence on the anisotropy of the collisions for rethermalization. For $\alpha = 0$ the collisions are isotropic and $\kappa \approx 2.1$. In comparison, $\kappa \approx 4.3$ at $\alpha = 1$, which describes the lowest partial wave scattering between identical fermions. For $E_c = 1 \mu\text{K}$ we find $\kappa \approx 9.7$, which is many times that for isotropic collisions, implying a significant increase in the number of collisions required for rethermalization. One may have anticipated this since the differential cross-section is more and more sharply peaked as α increases, and the energy is less

and less efficiently distributed. Also note that the outcome for the differential cross-section of KRb with $E_c = 1 \text{ nK}$ is very close to that from Eq. (10) with $\alpha = 1$, indicating that the lowest odd partial wave dominates for elastic collisions between fermions in indistinguishable internal and external state at ultra-low temperature.

C. Evaporation with anisotropic collisions

In evaporative cooling experiments, loss collisions compete with elastic collisions, and thus a slow thermalization rate gives rise to a reduction in cooling efficiency. In this section, we use MC simulations to investigate the efficiency of evaporative cooling in the presence of anisotropic elastic collisions, and also including two-body reactive collisions, as occur for KRb molecules. We quantify the efficiency in two ways: by the achieved increase in phase-space density Ω_t/Ω_0 at the expense of losing a certain portion of the molecules in the trap (see FIG. 2), and by the time required for the temperature to go down and Ω to increase by a given amount (see FIG. 3).

In these simulations, we assume an instantaneous removal of all particles with energy greater than a cut-off energy. The cut-off energy, ϵ_t , evolves during the evaporation trajectory with the constraint that a truncation parameter, $\eta = \epsilon_t/\bar{E}$, is kept constant, where \bar{E} is the average energy of the nonequilibrium distribution. The comparison between isotropic and anisotropic collisions is made by calculating the evaporation trajectory for a variety of differential cross-sections, starting with the same initial molecule number. To simplify the comparison, for both elastic and reactive collisions, we keep the total cross-sections constant and energy independent. More specifically, we consider elastic differential cross-sections in the form of Eq. (1), and choose the same $\lambda(E_c) = \lambda_{el}$ for

all differential cross-sections used in our simulations, leaving a, a', α and α' defined as in Table I ($a = 1, a' = \alpha = \alpha' = 0$ for isotropic collisions). And we fix the reactive cross-section via $\lambda_{re} = \zeta \lambda_{el}$, with ζ a constant ratio.

The molecules are initially simulated from a truncated Boltzmann distribution utilizing the cut-off energy [25] ϵ_t :

$$f(\mathbf{x}, \mathbf{p}) = n'_0 \exp\left(-\left(\frac{p^2}{m} + m\omega^2 x^2\right)/(2k_B T)\right) \times \Theta\left(\epsilon_t - \left(\frac{p^2}{2m} + \frac{1}{2}m\omega^2 x^2\right)\right), \quad (12)$$

where Θ is the Heaviside function, n'_0 is the normalization, and T is the initial temperature, held fixed for different simulations. Although the energy distribution of the molecules is intrinsically in nonequilibrium here, we may assign it a phase-space density, Ω , as that of the corresponding equilibrium distribution that has the same molecule number and average molecule energy.

In FIG. 2, Ω is plotted for the case of evaporation trajectories in which 90% of the initial molecules are lost. For anisotropic collisions, we calculate evaporation trajectories for the differential cross-sections for $E_c = 100$ nK and $E_c = 1\mu\text{K}$ given in the subsection II B. The results presented in FIG. 2 show that the maximum efficiency achievable by varying η is much lower for anisotropic collisions than that achievable with isotropic collisions. In addition, the maximum efficiency is reached at smaller η . This suggests, for example, that if ϵ_t is set by the trap depth in an experiment, a shallower trap is desirable for evaporating a gas with anisotropic collisions, compared with evaporating a gas with isotropic collisions, at the same temperature and collision rate.

For these calculations, the reactive to elastic collision rate ratio was held fixed at $\zeta = 1/200$. This was chosen based on typical experimental conditions for KRb molecules (see Sec. IV). The value of ζ does not qualitatively change the above comparisons; it only changes the shape of each curve [18], and as one would expect, the maximum efficiency and the corresponding η decreases as ζ increases.

In FIG. 3, we plot the time-dependent trajectories of evaporative cooling for isotropic collisions with $\eta = 4.3$, and for anisotropic collisions for $E_c = 1\mu\text{K}$ with $\eta = 3.3$. These values of η were chosen such that Ω_f/Ω_0 is maximum in FIG. 2, and thus most efficient. It is evident from this plot that to reach the same increase in Ω and decrease in T , it takes much shorter time with isotropic collisions (FIG. 3(b)). This indicates a lower efficiency with anisotropic collisions, consistent with the results of FIG. 2.

III. EVAPORATIVE COOLING IN 2D TRAPS

Physics in two-dimensional geometries can often be quite different from that in three-dimensions. Unlike many previous evaporative cooling experiments, KRb molecules need, in general, to be confined in traps with reduced dimensionality to be stable. Such a configuration was also used to evaporate Cs atoms [26]. Here, we study the effect of reduced dimen-

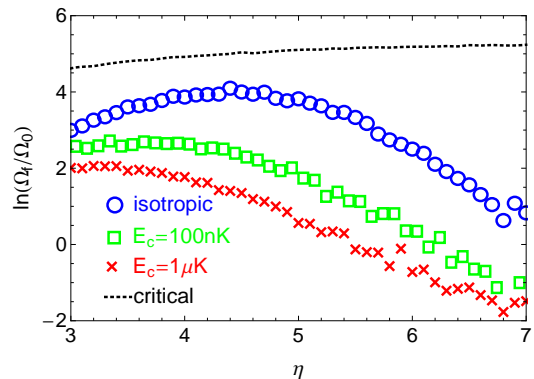


FIG. 2. (Color online) Increase in phase space density vs truncation parameter η for different $\frac{d\lambda(\phi)}{d\phi}$. Here Ω_0 is the initial phase space density, and the final phase space density, Ω_f , was calculated when the ratio of molecule numbers was $N_f/N_0 = 0.1$. Blue circles: $\frac{d\lambda(\phi)}{d\phi} = \text{const}$; red crosses: $(\frac{d\lambda(\phi)}{d\phi})_{E_c=1\mu\text{K}}$; green squares: $(\frac{d\lambda(\phi)}{d\phi})_{E_c=100\text{ nK}}$; black dotted line: critical phase space density Ω_c for quantum degeneracy.

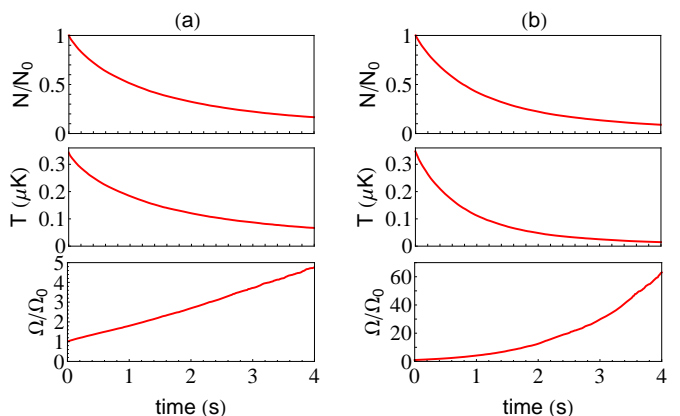


FIG. 3. (Color online) Trajectories of evaporation for (a): $(\frac{d\lambda(\phi)}{d\phi})_{E_c=1\mu\text{K}}$ at $\eta = 3.3$ and (b): $\frac{d\lambda(\phi)}{d\phi} = \text{const}$ at $\eta = 4.3$, under the same initial conditions as in FIG. 2. In comparison with (a), it is apparent that in (b) the temperature T drops faster and the phase-space density Ω increases much more rapidly.

sionality on evaporative cooling by comparing the efficiency in two-dimensional and three-dimensional traps.

The previous section showed that the existence of highly-anisotropic collisions slows down thermalization and decreases the efficiency of evaporative cooling. A calculation analogous to Sec. II B but for a three-dimensional harmonic trap gives

$$\kappa = \frac{5}{6}(2\alpha + 3), \quad (13)$$

which implies $\kappa = 2.5$ when $\alpha = 0$ (isotropic collisions). This result may suggest a potentially faster thermalization rate and more efficient evaporation in a two-dimensional harmonic

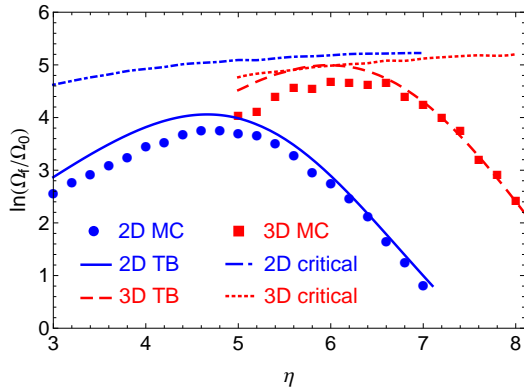


FIG. 4. (Color online) Comparison of the efficiency of evaporative cooling in two-dimensional (2D) and three-dimensional (3D) harmonic traps. $\ln(\Omega_f/\Omega_0)$'s are calculated at $N_f/N_0 = 0.1$, and $\zeta = 1/200$. Red (blue) line: 3D (2D) harmonic trap from method in Appendix C; red squares: 3D harmonic trap from MC simulation; blue disks: 2D harmonic trap from MC simulation; blue (red) dotted line: Ω_c for a 2D (3D) trap.

trap when compared with a three-dimensional harmonic trap with everything else held fixed. However, such a conclusion based solely on Eq. (13) would be premature, since the density of states depends on the dimensionality. Specifically, it was found for the comparison between quadratic potentials and linear potentials in three dimensions that changing the density of states can also change the evaporative cooling efficiency [18].

To incorporate such differences, we use MC simulation and a truncated-Boltzmann (TB) method based on kinetic theory (see Appendix C) to calculate the evaporation trajectories. Here, we consider harmonic traps and isotropic energy-independent collisions in order to isolate the effect of dimensionality. Following a similar procedure to that of the previous section, we calculate $\ln(\Omega_f/\Omega_0)$ at fixed N_f/N_0 , under equivalent initial conditions for both types of traps. As shown in FIG. 4, both the MC and TB approaches show a lower achievable increase in the phase-space density for a two-dimensional harmonic trap. This suggests that evaporative cooling is intrinsically less efficient in two-dimensional traps. The discrepancy between MC and TB, which increases for smaller η , is caused by the discrepancy between the form of the energy distributions, which for TB is constrained. At smaller η , the truncated Boltzmann distribution deviates significantly from the actual distribution of molecules, as calculated in MC.

IV. EVAPORATIVE COOLING OF KRB MOLECULES

In a quasi-two-dimensional trap, the elastic and reactive collisions between KRb molecules both depend on both the strength of the external electric field and the confinement induced by the lattice. Under current trapping conditions in experiments, a favorable ratio between the elastic and reactive processes can be reached at a moderate electric field [15–

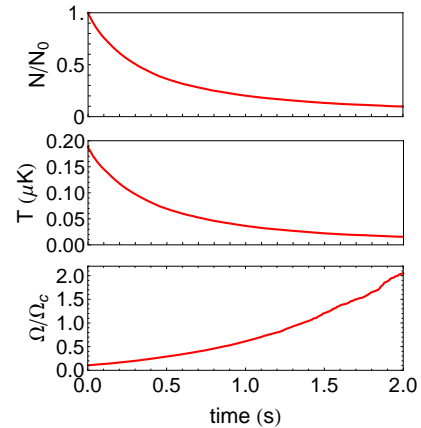


FIG. 5. (Color online) Evaporative cooling trajectories for KRb molecules inside a 2D trap of $2\pi \times 20$ Hz, with scattering cross-sections as computed in FIG. 1(b). The initial temperature was ~ 200 nK, with an initial phase-space density $\Omega_0 \sim 0.1\Omega_c$, and $\eta = 3.8$.

17]. We show in FIG. 1(b) the total scattering cross-section for the elastic process and reactive process of KRb molecules at $d = 0.2$ debye with the confinement along the lattice direction given by $\nu = 23$ kHz. In the ultracold regime, the elastic cross-section scales as $E_c^{3/2}$, while the reactive cross-section scales as $E_c^{1/2}$ [27]. Furthermore, elastic processes are found to be generally faster than reactive processes, supporting the potential for successful evaporative cooling [17] while the large elastic cross-section favors fast rethermalization. The quantitative knowledge of the elastic and reactive collisions between KRb molecules allows us to apply MC simulation with realistic experimental parameters. In FIG. 5, we show evaporation trajectories in a $2\pi \times 20$ Hz two-dimensional gaussian trap. For this simulation, we have assumed the instantaneous removal of energetic molecules above the cut, as in Sec. II C and Sec. III. We also assume reactive losses as discussed above. The initial temperature was chosen to be within the accessible regime of experiments. The results show that a considerable increase in phase-space density can be achieved via evaporative cooling. We note that there are further experimental effects that can in principle reduce the achieved phase-space density increase from that calculated here, such as the finite rate of removing energetic molecules and other sources of loss and heating. On the other hand, progress towards realizing deeper lattices (*i.e.*, $\nu > 23$ kHz), can potentially reduce ζ and thereby enhance the cooling efficiency.

V. ANTI-EVAPORATION IN QUASI-2D

Fast reactive collisions are disadvantageous for evaporative cooling, since they not only reduce the molecule number, but can also cause heating known as “anti-evaporation” [10]. Since the ability to identify the relative importance of different heating mechanisms is important in the design of experi-

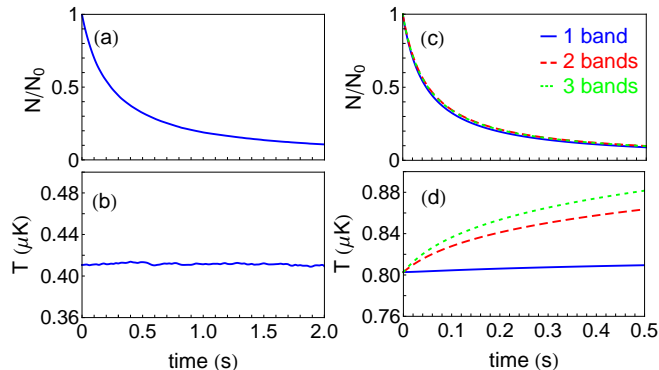


FIG. 6. (Color online) Heating due to two-body losses in a two-dimensional harmonic trap. Here (a) and (b) show the MC result in a two-dimensional harmonic trap where all molecules are in the lowest band of the lattice potential. The results for (c) and (d) are obtained with the master equation approach. The blue line assumes only 1 band along the lattice direction is populated. The red dashed line (green dots) assumes 2 (3) bands are populated. N_0 is the initial total molecule number. The initial temperature is chosen to be around 800 nK, so that when two bands are included, there are $\sim 25\%$ of molecules on the second band, and when three bands are included, there are $\sim 19\%$ of molecules on the second band and $\sim 6\%$ on the third band.

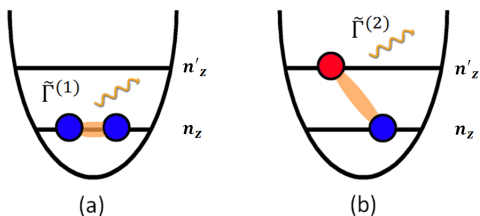


FIG. 7. (Color online) Collisions between molecules in a quasi-2D trap. (a) Intra-band collisions, occurring at rate $\tilde{\Gamma}^{(1)}$. (b) Inter-band collisions, occurring at rate $\tilde{\Gamma}^{(2)}$ (see Appendix D). The wavy arrows indicate that the molecules are lost from the trap after these reactive collisions.

ments, in this section we quantitatively investigate heating due to two-body reactive collisions.

Anti-evaporation arises from the fact that reactive collisions are more frequent in the high density region of the trap (density-selection). Molecules there have on average total energies that are less than the ensemble average. Thus one may anticipate evaporative heating rather than evaporative cooling to occur. In competition with this, however, is the effect that the reactive collision cross-section is dependent on the collision energy, *i.e.*, molecules with energies higher than the average are more likely to engage in a reactive collision and be removed (velocity-selection). In three-dimensional harmonic traps, the reactive processes for ultracold indistinguishable fermionic KRb molecules are mainly p -wave two-body collisions, the cross-section of which scales as $E_c^{1/2}$ [10]. The

density-selection mechanism wins over the velocity-selection mechanism and consequently there is net heating induced by losses [10]. In two-dimensional trapping potentials, however, this is not necessarily true even though the cross-section scales similarly with E_c (see Sec. IV), as we now show.

We consider a two-dimensional harmonic trap and assume a Boltzmann distribution as given in Eq. (3), for which the number loss rate is

$$\frac{dN}{dt} = -2 \int d^2x d^2p_1 d^2p_2 \lambda(E_{\text{rel}}) v_{\text{rel}} f_0(\mathbf{x}, \mathbf{p}_1) f_0(\mathbf{x}, \mathbf{p}_2), \quad (14)$$

and the corresponding energy loss is

$$\frac{dE}{dt} = - \int d^2x d^2p_1 d^2p_2 \lambda(E_{\text{rel}}) v_{\text{rel}} f_0(\mathbf{x}, \mathbf{p}_1) f_0(\mathbf{x}, \mathbf{p}_2) (E_1 + E_2), \quad (15)$$

where E_{rel} and v_{rel} are the relative energy and velocity between the two colliding molecules, and $E_1 + E_2$ is the total energy. From Eq. (14) and Eq. (15), with $\lambda(E_{\text{rel}}) \propto E^{1/2}$ (see Sec. IV), one can derive the energy loss per molecule, which is given by

$$\frac{dE}{dN} = 2k_B T. \quad (16)$$

This implies that there is no net heating or cooling in a pure two-dimensional harmonic trap due to reactive loss. This is because the energy loss in a single reactive process is exactly the average energy for a pair of molecules. In contrast, a similar calculation for three-dimensional harmonic traps gives $dE/dN = 2.75k_B T$, which is smaller than the average energy per molecule (*i.e.* $3k_B T$), indicating heating in that case. This conclusion for three-dimensional traps is consistent with the experimental observation in Ref. [10] (heating rate ~ 100 nK/s).

However, we emphasize that Eq. (14) to Eq. (16) only takes into account the two-body reactive collisions and assumes a Boltzmann distribution, which implies sufficiently fast rethermalization. Note that at zero electric field, the elastic collisions that lead to thermalization are infrequent and can generally be neglected in experiments with KRb molecules [10], thus a Boltzmann distribution is not guaranteed.

To study possible effects caused by the deviation from a Boltzmann distribution during the evolution, we use MC simulations to calculate the molecule loss and temperature change in a two-dimensional harmonic trap, assuming only two-body reactive processes between molecules. The results are plotted in FIGs. 6(a) and (b) respectively. The reactive collision rate is taken from FIG. 1 (b). The heating rate is found to be very small, illustrating a drastically different quantitative behavior from that seen in three-dimensional traps.

The periodic array of two-dimensional pancake traps for confining KRb molecules is generated by a one-dimensional optical lattice [15]. This forms energy bands separated by $\sim \hbar\omega_z$, where $\omega_z = 2\pi\nu$ and ν is the frequency of the harmonic approximation of the lattice potential. When the temperature is sufficiently low, the longitudinal degree-of-freedom along the lattice axis is effectively frozen out and one may consider

solely the lowest band. However, as the temperature increases, higher bands can be populated. For example, at $T \sim 800$ nK in a lattice of $\nu = 23$ kHz, about 25% of molecules occupy higher bands.

With multiband population, collisions between molecules can occur as inter-band or intra-band, as shown in FIG. 7. The inter-band collisions involve additional degrees-of-freedom along the longitudinal direction (see FIG. 7(b)), and thus do not satisfy the assumptions leading to Eq. (16) and can give rise to anti-evaporation heating [10].

In the ultra-low temperature regime, these collisions are dominated by the lowest odd partial wave [10]. We adopt a p -wave many-body Hamiltonian to describe such reactive interactions [28–30]:

$$\hat{H}_p = \frac{3\pi b_p^3 \hbar^2}{m} \int d^3r [(\nabla \hat{\Psi}^\dagger(\mathbf{r})) \hat{\Psi}^\dagger(\mathbf{r}) - \hat{\Psi}^\dagger(\mathbf{r})(\nabla \hat{\Psi}^\dagger(\mathbf{r}))] \cdot [(\nabla \hat{\Psi}(\mathbf{r})) \hat{\Psi}(\mathbf{r}) - \hat{\Psi}(\mathbf{r})(\nabla \hat{\Psi}(\mathbf{r}))], \quad (17)$$

where $\hat{\Psi}(\mathbf{r})$ is a fermionic field operator that annihilates a molecule at position \mathbf{r} , and b_p^3 is the p -wave inelastic scattering volume. The value of b_p for KRb molecules can be found from the reactive cross-section calculated in the previous section. In a trap with transverse confinement ω_r and longitudinal confinement ω_z , the field operator can be expanded in the basis of non-interacting harmonic oscillator eigenstates ψ_n^r (corresponding to ω_r) and ψ_n^z (corresponding to ω_z) as:

$$\hat{\Psi}(\mathbf{r}) = \sum_{\mathbf{n}} \hat{c}_{\mathbf{n}} \psi_{n_x}^r(x) \psi_{n_y}^r(y) \psi_{n_z}^z(z), \quad (18)$$

where $\mathbf{n} = (n_x, n_y, n_z)$ enumerates the mode number along each dimension, and $\hat{c}_{\mathbf{n}}$ annihilates a fermion in mode \mathbf{n} .

Considering elastic collisions to be negligible, we assume there is no change of modes during the losses, *i.e.*, a molecule initially in mode \mathbf{n} remains in mode \mathbf{n} . With such an assumption, each molecule can be labeled with its mode indices, and for identical fermions, there are no two molecules with the same indices. The two-body losses can then be accounted for by jump operators $\hat{A}_{\mathbf{n},\mathbf{m}} = \sqrt{\Gamma_{\mathbf{n},\mathbf{m}}} \hat{c}_{\mathbf{n}} \hat{c}_{\mathbf{m}}$, which remove two molecules in mode \mathbf{n} and \mathbf{m} at a rate $\Gamma_{\mathbf{n},\mathbf{m}}$ determined by the corresponding p -wave two-body reactive collisions Eq. (17) (see Appendix D for details). When $n_z = m_z$, these correspond to the intra-band collisions (FIG. 7(a)); when $n_z \neq m_z$, these correspond to the inter-band collisions (FIG. 7(b)).

The dynamics can then be described by the quantum master equation

$$\frac{d\hat{\rho}}{dt} = \frac{1}{2} \sum_{\mathbf{n},\mathbf{m}} (2\hat{A}_{\mathbf{n},\mathbf{m}} \hat{\rho} \hat{A}_{\mathbf{n},\mathbf{m}}^\dagger - \hat{A}_{\mathbf{n},\mathbf{m}}^\dagger \hat{A}_{\mathbf{n},\mathbf{m}} \hat{\rho} - \hat{\rho} \hat{A}_{\mathbf{n},\mathbf{m}}^\dagger \hat{A}_{\mathbf{n},\mathbf{m}}). \quad (19)$$

Since we have assumed that the molecules do not change modes during evolution, in order to solve Eq. (19), we can use $\hat{\rho} = \prod_i \sum_{\mathbf{n}} \rho_{\mathbf{n},\mathbf{n}}^i \delta(\mathbf{n} - \mathbf{n}^i) |\mathbf{n}\rangle \langle \mathbf{n}|$, where $i = 1, 2, 3 \dots N$ represents the i th molecule that initially is in mode \mathbf{n}^i , N is the initial total number of molecules. Since the quantum jumps here correspond to the reactive loss of pairs of molecules, the off-diagonal coherence terms have been dropped. The rele-

vant equation of motion under these assumptions is

$$\frac{d\rho_{\mathbf{n}^i, \mathbf{n}^i}^i}{dt} = -\rho_{\mathbf{n}^i, \mathbf{n}^i}^i \sum_{j \neq i} \Gamma_{\mathbf{n}^i, \mathbf{m}^j} \rho_{\mathbf{m}^j, \mathbf{m}^j}^j. \quad (20)$$

The total molecule number at time t is thus

$$N(t) = \sum_i \rho_{\mathbf{n}^i, \mathbf{n}^i}^i(t), \quad (21)$$

and the average temperature can be found from

$$T(t) = \frac{1}{N(t) k_B} \sum_i \hbar \omega_r (n_x^i + n_y^i) \rho_{\mathbf{n}^i, \mathbf{n}^i}^i(t). \quad (22)$$

Furthermore, the initial population in different bands can be determined by

$$\frac{N^\alpha}{N} = \frac{e^{-(1/2 + \alpha \hbar \omega_z)/k_B T}}{\sum_\alpha e^{-(1/2 + \alpha \hbar \omega_z)/k_B T}}, \quad (23)$$

where $\alpha = 0, 1, \dots$ is the band index. For the initial condition, the density matrix is simulated such that N^α molecules are assigned to band index $n_z = \alpha$, and the transverse modes n_x^i, n_y^i are randomly generated from a Boltzmann distribution with given initial temperature T . The final result is averaged over many different simulations. In order to show the effect of including different number of bands, we assume a cut-off in the highest band index. In our calculation, if a total of n_{max} bands are taken into account, the population of the lower $n_{max} - 2$ bands is determined according to Eq. (23). All of the reminder molecules are assigned to the highest populated band, $n_{max} - 1$.

In FIG. 6(c) and (d), we show the result with temperature $T = 800$ nK and lattice frequency $\nu = 23$ kHz, which are typical for KRb experiments. While the small amount of multiband population does not lead to a significant change in the loss rate for molecules (FIG. 6(c)), there can nevertheless be significant heating. In consequence, it is necessary to greatly suppress the population outside the lowest band for evaporative cooling experiments to be effectively performed in quasi-two-dimensional geometries when reactive loss of the form considered here is present.

VI. CONCLUSION

Motivated by recent experiments of KRb molecules, we have applied MC simulation methods and semianalytical approaches to perform a detailed study of evaporative cooling properties in two-dimensional traps with anisotropic collisions. We have quantitatively analyzed the dependence of the thermalization rate on the anisotropy of the elastic collisions. Specifically, for our calculations of the differential and total scattering cross-section for KRb molecules confined in a quasi-two-dimensional trap, we were able to investigate the efficiency of evaporative cooling for the practical parameter regime of recent experiments. The dipole-dipole interactions resulted in highly anisotropic elastic collisions which

were disadvantageous for evaporative cooling when compared with isotropic collisions.

The reduced dimension of the trapping potential further decreased the efficiency of evaporative cooling when compared with conventional evaporation procedures for three-dimensional traps. Nevertheless, we showed that the phase space density of KRb molecules can potentially be increased using evaporative cooling with parameters that are accessible under current experimental conditions. Although this could be limited by further complicated real-world experimental details that we have not considered, it is also the case that future experimental progress in increasing the ratio between the elastic and reactive collision rates could lead to more efficient evaporative cooling of KRb molecules.

We also developed theoretical models to investigate the anti-evaporation induced by two-body losses. Our results highlighted the distinctions between the evaporation processes in two-dimensional and three-dimensional geometries through the role of multiband excitations in a quasi-two-dimensional trap. We point out that the importance of multi-band physics has also been addressed in recent literature [31–33].

ACKNOWLEDGMENTS

We would like to thank the JILA KRb group, John Bohn, Kaden Hazzard and Alexander Pikovski for helpful discussions. We acknowledge support from ARO, AFOSR, NSF-PIF, NSF JILA-PFC-1125844, NIST, and ARO-DARPA-OLE.

Appendix A: Scattering cross-section in a quasi-2D trap

Here we outline the theoretical formalism we used to compute the total and differential scattering cross-sections in a two-dimensional space, for elastic and reactive processes of KRb+KRb collisions, in the presence of an electric field along the confinement direction. More details can also be found in Ref. [16].

We use a time-independent scattering formalism based on Jacobi coordinates. The KRb molecules are assumed to be in their ground electronic, vibrational and rotational states. They are also assumed to be in the ground state of the one dimensional optical lattice. The results of this formalism compare well with experimental observation [15]. The vector \mathbf{r} represents the relative distance between the two centers of mass of the two molecules. The potential energy between the two molecules is given by the van der Waals interaction and the dipole-dipole interaction that arises in the presence of an external applied electric field. In addition to the intermolecular interaction potential, each molecule feels a one dimensional confining potential approximated by an harmonic oscillator. At short range, we apply an absorbing potential that takes into account the fact that the KRb molecules are chemically reactive and are lost from the trap.

The time-independent Schrödinger equation is solved for each intermolecular separation r using a spherical representation of $\mathbf{r} = (r, \theta, \phi)$. At long distance, the van der Waals and dipolar interactions vanish while the confinement is still present. It is therefore more convenient to use a cylindrical representation of $\mathbf{r} = (\rho, \phi, z)$. Since the electric field and the confinement axis of the optical lattice are parallel to the quantization axis, the quantum number m_l associated with the projection of the orbital angular momentum is strictly conserved during the collision. Since we assume that the fermionic KRb molecules, all in the same internal ground state, are also in the same external ground state of the optical lattice, the quantum number m_l is restricted to odd values $m_l = \pm 1, \pm 3, \pm 5, \dots$ [16]. A frame transformation is performed at long range between the two representations. Applying asymptotic boundary conditions at long range, we obtain the scattering matrix S^{m_l} and the transition matrix $T^{m_l} = S^{m_l} - 1$.

The elastic differential cross-section for initial and final KRb molecules in the internal and external ground state is given by [34]:

$$\frac{d\lambda(\phi)}{d\phi} = |f_s(\phi)|^2 \quad (\text{A1})$$

where the scattering amplitude is:

$$f_s(\phi) = \left(\frac{1}{2\pi i k} \right)^{1/2} \sum_{m_l=1,3,\dots}^{\infty} \epsilon_{m_l} \cos(m_l \phi) T^{m_l} \Delta \quad (\text{A2})$$

with $k = \sqrt{2\mu E_c}/\hbar$ denoting the wavevector, E_c the collision energy, μ the reduced mass of the colliding pair, $\epsilon_{m_l} = 2$ if $m_l \geq 1$, $\epsilon = 1$ if $m_l = 0$, and $\Delta = 2$ or 1 if the molecules are indistinguishable or not. To converge the results, we used 10 odd values of m_l , with $m_l = [1, 3, \dots, 19]$. The total elastic cross-section is given by:

$$\lambda = \int_0^{2\pi} d\phi \frac{d\lambda(\phi)}{d\phi}. \quad (\text{A3})$$

As seen from the differential cross-section shown in FIG. 1(a), scattering in the perpendicular direction is forbidden. This is due to the $\cos(m_l \phi)$ term, with the odd m_l restriction arising from the fermionic indistinguishable character of the molecules.

Appendix B: Monte Carlo simulation

With its stochastic nature, the Monte Carlo method is capable of simulating the individual collisions that are intrinsic to evaporative cooling phenomena [22, 35, 36], and this leads to a flexible algorithm in which it is easy to incorporate a variety of different conditions in a straightforward way. The detailed simulation algorithm consists mainly of the following steps:

1. Preparation of an ensemble of particles with coordinates and velocities generated from a given probability distribution, e.g. an initial equilibrium Boltzmann distribution.

2. Evolution of the particles between collisions that follows the classical Hamilton's equations of motion, *i.e.*

$$\begin{aligned}\frac{d\mathbf{x}}{dt} &= \mathbf{v}, \\ \frac{d\mathbf{v}}{dt} &= -\nabla V(\mathbf{x}),\end{aligned}\quad (\text{B1})$$

where $V(\mathbf{x})$ is the external potential. The time step is chosen to be both small enough to guarantee numerical convergence for the computed trajectory, as well as much less than the time between adjacent collision events.

3. Checking every pair of particles to decide if there is a collision. Since we are interested in two-body collisions, the collision events are determined by the distance between particles. This distance is characterized by the scattering length a_s . In three-dimensional collisions, there is a collision cross-section with units of area, $\sigma = \pi a_s^2$. In two-dimensional collisions, there is an analogous cross-section with units of length, $\lambda = 2a_s$.

4. Changing the state of the pair of particles if they collide. For an elastic collision event, the velocities after collisions are determined from the conservation of total momentum and energy. The scattering angle is simulated from a probability distribution determined by the differential cross-section. For instance, in two-dimensional s -wave scattering, the outgoing angles ϕ are uniformly distributed in the interval $[0, 2\pi)$, while for p -wave scattering, the distribution of the outgoing angles follows the distribution $\cos^2\phi$. In three-dimensional isotropic scattering, there are two random angles: an azimuthal angle ϕ uniformly distributed in the interval $[0, 2\pi)$ and a polar angle θ from uniformly distributed according to $\cos\theta$. The non-uniform distribution of the scattering angles does not affect the collision rate that is determined by the total cross-section, but the rate of redistributing energies does vary. For a loss event corresponding to two-body reactive collision, the two particles are lost from the trap after the collision, and thus deleted from the simulation when such processes occur.

5. Averaging over many initial samples and trajectories. The physical quantities such as the total number of particles, temperature, collision rate and phase space density can be computed statistically from the simulation ensemble.

Appendix C: Kinetics of evaporative cooling in 2D

An alternative algorithm which is partially analytic can be derived by assuming that in the process of evaporative cooling, the energetic particles can be efficiently removed from the trap. The system is assumed to follow a truncated Boltzmann distribution $f(\mathbf{x}, \mathbf{p})$ (Eq. 12), with a cut-off energy ϵ_t [25, 37], meaning that there is no particle with energy $E > \epsilon_t$. Then similar to the description of an equilibrium ensemble, the measured quantities of the system can be expressed by averaging over this distribution function. For example, the collision rate is

$$\gamma = \frac{\lambda\Lambda^2}{m} \int_{\epsilon_1, \epsilon_2} d^2x d^2p_1 d^2p_2$$

$$\times f(\mathbf{x}, \mathbf{p}_1) f(\mathbf{x}, \mathbf{p}_2) |\mathbf{p}_1 - \mathbf{p}_2|, \quad (\text{C1})$$

in which $\Lambda = 1/(2\pi\hbar)^2$, and $\epsilon_{1,2} = p_{1,2}^2/2m + V(\mathbf{x}_{1,2})$ are the energies of the incident particles. For simplicity, here we have assumed isotropic energy-independent elastic and reactive collisions, so λ in Eq. (C1) is constant. We also assume the two-body reactive collisions happen at rate $\zeta\gamma$. During forced evaporative cooling, ϵ_t decreases with time, so does the temperature T , and the distribution function $f = f(\mathbf{x}, \mathbf{p})$. As a result, the evolution of the system from t to t' can be modeled via three steps: the change due to f when ϵ_t decreases to ϵ'_t (dN_1, dE_1), the change due to evaporation (dN_2, dE_2), and the change due to the reactive losses (dN_3, dE_3). These can be represented by the following equations:

$$dN_1 = \Lambda \int_{\epsilon=\epsilon'_t}^{\epsilon_t} d^2x d^2p f, \quad (\text{C2})$$

$$dE_1 = \Lambda \int_{\epsilon=\epsilon'_t}^{\epsilon_t} d^2x d^2p \epsilon f, \quad (\text{C3})$$

$$\frac{dN_2}{dt} = \frac{\lambda\Lambda^2}{m} \int_{\Sigma} d^2x d^2p_1 d^2p_2 d\phi' f_1 f_2 |\mathbf{p}_1 - \mathbf{p}_2|, \quad (\text{C4})$$

$$\frac{dE_2}{dt} = \frac{\lambda\Lambda^2}{m} \int_{\Sigma} d^2x d^2p_1 d^2p_2 d\phi' s f_1 f_2 |\mathbf{p}_1 - \mathbf{p}_2| \epsilon_4, \quad (\text{C5})$$

$$\frac{dN_3}{dt} = \zeta \frac{\lambda\Lambda^2}{m} \int_{\Sigma'} d^2x d^2p_1 d^2p_2 f_1 f_2 |\mathbf{p}_1 - \mathbf{p}_2|, \quad (\text{C6})$$

$$\frac{dE_3}{dt} = \zeta \frac{\lambda\Lambda^2}{m} \int_{\Sigma'} d^2x d^2p_1 d^2p_2 f_1 f_2 |\mathbf{p}_1 - \mathbf{p}_2| (\epsilon_1 + \epsilon_2), \quad (\text{C7})$$

where f_1, f_2 are the distribution function for each of the two colliding particles, ϕ' specifies the scattering angle, $\epsilon = \epsilon(\mathbf{x}, \mathbf{p})$ is the energy of a particle and is a function of the coordinate and momentum of the particles, ϵ_3 and ϵ_4 are energies after collision, which are determined once $\mathbf{p}_1, \mathbf{p}_2$ and ϕ' are known, and $\Sigma = \{\epsilon_1, \epsilon_2, \epsilon_3 < \epsilon'_t, \epsilon_4 > \epsilon'_t\}$ and $\Sigma' = \{\epsilon_1, \epsilon_2 < \epsilon'_t\}$ specify the integration region. These contributions add up to give the total changes: $N(t') = N(t) - dN_1 - dN_2 - dN_3$ and $E(t') = E(t) - dE_1 - dE_2 - dE_3$. The new temperature $T(t')$ is found from

$$N(t') = \Lambda \int_0^{\epsilon'_t} d^2x d^2p f(\mathbf{x}, \mathbf{p}), \quad (\text{C8})$$

$$E(t') = \Lambda \int_0^{\epsilon'_t} d^2x d^2p f(\mathbf{x}, \mathbf{p}) \epsilon. \quad (\text{C9})$$

Then the trajectory of evaporative cooling in two-dimensional traps can be solved from the above equations. Similar calculations also apply to three-dimensional harmonic traps, and the results are equivalent to solving the rate equations following the method developed by Walraven *et al.*, as long as the truncated Boltzmann distribution is a good approximation [25].

Appendix D: Master equation approach for losses in a quasi-2D trap

Represented in the basis of harmonic oscillator eigenstates, the rate coefficients $\Gamma_{\mathbf{n},\mathbf{m}}$ defined in the jump operators in Sec. V can be written explicitly for intra-band collisions ($n_z = m_z$, FIG. 7(a)) [30]

$$\begin{aligned} \Gamma_{\mathbf{n},\mathbf{m}} &= \tilde{\Gamma}^{(1)} \\ &= \frac{3\sqrt{2\pi}b_p^3\sqrt{\omega_r\omega_z}}{a_{\text{rho}}^3} I_s(n_z, m_z, n_z, m_z) \\ &\quad \times \sum_{\sigma \neq \sigma'} I_s(n_\sigma, m_\sigma, n_\sigma, m_\sigma) I_p(n_{\sigma'}, m_{\sigma'}, n_{\sigma'}, m_{\sigma'}), \end{aligned} \quad (\text{D1})$$

and for inter-band collisions ($n_z \neq m_z$, FIG. 7(b))

$$\begin{aligned} \Gamma_{\mathbf{n},\mathbf{m}} &= \tilde{\Gamma}^{(2)} \\ &= \frac{3\sqrt{2\pi}b_p^3\sqrt{\omega_r\omega_z}}{a_{\text{rho}}^3} \sum_{\sigma_1 \neq \sigma_2 \neq \sigma_3} \frac{\omega_{\sigma_2}}{\omega_r} I_s(n_{\sigma_1}, m_{\sigma_1}, n_{\sigma_1}, m_{\sigma_1}) \end{aligned}$$

$$\times I_p(n_{\sigma_2}, m_{\sigma_2}, n_{\sigma_2}, m_{\sigma_2}) I_s(n_{\sigma_3}, m_{\sigma_3}, n_{\sigma_3}, m_{\sigma_3}), \quad (\text{D2})$$

where $\sigma, \sigma' = \{x, y\}$, $\sigma_1, \sigma_2, \sigma_3 = \{x, y, z\}$, $a_{\text{rho}} = \sqrt{\hbar/m\omega_r}$,

$$I_s(n, m, p, q) = \int du \frac{e^{-2u^2} H_n(u) H_m(u) H_p(u) H_q(u)}{\pi \sqrt{2^{n+m+p+q} n! m! p! q!}}, \quad (\text{D3})$$

$$\begin{aligned} I_p(n, m, p, q) &= \int du \frac{e^{-2u^2}}{\pi \sqrt{2^{n+m+p+q} n! m! p! q!}} \\ &\quad \times [\partial H_n(u) H_m(u) - H_n(u) \partial H_m(u)] \\ &\quad \times [\partial H_p(u) H_q(u) - H_p(u) \partial H_q(u)], \end{aligned} \quad (\text{D4})$$

and H_n, H_m, H_p, H_q are Hermite polynomials.

-
- [1] T. Lahaye, C. Menotti, L. Santos, M. Lewenstein, and T. Pfau, Rep. Prog. Phys. **72**, 126401 (2009).
 - [2] P. G. H. Sandars, Phys. Rev. Lett. **19**, 1396 (1967).
 - [3] E. R. Hudson, H. J. Lewandowski, B. C. Sawyer, and J. Ye, Phys. Rev. Lett. **96**, 143004 (2006).
 - [4] S. F. Yelin, K. Kirby, and R. Côté, Phys. Rev. A **74**, 050301 (2006).
 - [5] D. DeMille, Phys. Rev. Lett. **88**, 067901 (2002).
 - [6] A. Micheli, G. Brennen, and P. Zoller, Nature Physics **2**, 341 (2006).
 - [7] L. Carr, D. DeMille, R. Krems, and J. Ye, New Journal of Physics **11**, 055049 (2009).
 - [8] K. Ni, S. Ospelkaus, M. De Miranda, A. Pe'er, B. Neyenhuis, J. Zirbel, S. Kotochigova, P. Julienne, D. Jin, and J. Ye, science **322**, 231 (2008).
 - [9] S. Ospelkaus, K. Ni, M. De Miranda, B. Neyenhuis, D. Wang, S. Kotochigova, P. Julienne, D. Jin, and J. Ye, Faraday Discussions **142**, 351 (2009).
 - [10] K. Ni, S. Ospelkaus, D. Wang, G. Quémener, B. Neyenhuis, M. De Miranda, J. Bohn, J. Ye, and D. Jin, Nature **464**, 1324 (2010).
 - [11] C. C. Bradley, C. A. Sackett, J. J. Tollett, and R. G. Hulet, Phys. Rev. Lett. **75**, 1687 (1995).
 - [12] K. B. Davis, M. O. Mewes, M. R. Andrews, N. J. van Druten, D. S. Durfee, D. M. Kurn, and W. Ketterle, Phys. Rev. Lett. **75**, 3969 (1995).
 - [13] B. DeMarco and D. Jin, Science **285**, 1703 (1999).
 - [14] G. Quémener and J. L. Bohn, Phys. Rev. A **81**, 022702 (2010).
 - [15] M. de Miranda, A. Chotia, B. Neyenhuis, D. Wang, G. Quémener, S. Ospelkaus, J. Bohn, J. Ye, and D. Jin, Nature Physics **7**, 502 (2011).
 - [16] G. Quémener and J. L. Bohn, Phys. Rev. A **83**, 012705 (2011).
 - [17] G. Quémener and J. L. Bohn, Phys. Rev. A **81**, 060701 (2010).
 - [18] W. Ketterle and N. Druten, Advances in atomic, molecular, and optical physics **37**, 181 (1996).
 - [19] M. R. Gochitashvili, R. Y. Kezerashvili, and R. A. Lomsadze, Phys. Rev. A **82**, 022702 (2010).
 - [20] Note: The cross-section in two-dimensions has a dimension of length.
 - [21] C. R. Monroe, E. A. Cornell, C. A. Sackett, C. J. Myatt, and C. E. Wieman, Phys. Rev. Lett. **70**, 414 (1993).
 - [22] B. DeMarco, J. L. Bohn, J. P. Burke, M. Holland, and D. S. Jin, Phys. Rev. Lett. **82**, 4208 (1999).
 - [23] F. Reif, *Fundamentals of statistical and thermal physics*, McGraw-Hill series in fundamentals of physics (McGraw-Hill, 1965).
 - [24] J. L. Roberts, N. R. Claussen, J. P. Burke, C. H. Greene, E. A. Cornell, and C. E. Wieman, Phys. Rev. Lett. **81**, 5109 (1998).
 - [25] O. J. Luiten, M. W. Reynolds, and J. T. M. Walraven, Phys. Rev. A **53**, 381 (1996).
 - [26] C.-L. Hung, X. Zhang, N. Gemelke, and C. Chin, Physical Review A **78**, 011604 (2008).
 - [27] Z. Li, S. V. Alyabyshev, and R. V. Krems, Phys. Rev. Lett. **100**, 073202 (2008).
 - [28] K. Kanjilal and D. Blume, Phys. Rev. A **70**, 042709 (2004).
 - [29] M. D. Swallows, M. Bishof, Y. Lin, S. Blatt, M. J. Martin, A. M. Rey, and J. Ye, science **331**, 1043 (2011).
 - [30] M. J. Martin, M. Bishof, M. D. Swallows, X. Zhang, C. Benko, J. von Stecher, A. V. Gorshkov, A. M. Rey, and J. Ye, Science **341**, 632 (2013).
 - [31] P. Soltan-Panahi, D.-S. Lühmann, J. Struck, P. Windpassinger, and K. Sengstock, Nature Physics **8**, 71 (2011).
 - [32] M. J. Mark, E. Haller, K. Lauber, J. G. Danzl, A. J. Daley, and H.-C. Nägerl, Phys. Rev. Lett. **107**, 175301 (2011).
 - [33] S. Will, T. Best, U. Schneider, L. Hackermüller, D.-S. Lühmann, and I. Bloch, Nature **465**, 197 (2010).
 - [34] I. R. Lapidus, American Journal of Physics **50**, 45 (1982).
 - [35] H. Wu and C. J. Foot, Journal of Physics B: Atomic, Molecular and Optical Physics **29**, L321 (1996).
 - [36] H. Wu, E. Arimondo, and C. J. Foot, Phys. Rev. A **56**, 560 (1997).
 - [37] M. J. Holland, B. DeMarco, and D. S. Jin, Phys. Rev. A **61**, 053610 (2000).